Assessment of Cholesterol Homeostasis in the Living Human Brain

Ahmed Haider[1,2†], Chunyu Zhao[1,2†], Lu Wang[3†], Zhiwei Xiao[1,2], Jian Rong[1,2], Xiaotian Xia[1,4], Zhen Chen[1], Stefanie K. Pfister[1], Natalia Mast[5], Eylan Yutuc[6], Jiahui Chen[1,2], Yinlong Li[1,2], Tuo Shao[1], Geoffrey I. Warnock[7,8], Alyaa Dawoud[9], Theresa R. Connors[10,11], Derek H. Oakley[10,12,13,14,15], Huiyi Wei[3], Jinghao Wang[16], Zhihua Zheng[17], Hao Xu[3], April T. Davenport[18], James B. Daunais[18], Richard S. Van[19], Yihan Shao[19], Yuqin Wang[6], Ming-Rong Zhang[20], Catherine Gebhard[7,8], Irina Pikuleva[5], Allan I. Levey[21], William J. Griffiths[6], Steven H. Liang[1,2*]

*Corresponding author. Email: steven.liang@emory.edu

Supporting Information

This PDF file includes:

Materials and Methods

All chemicals used in the synthesis of CHL-2205 and the corresponding precursor were directly acquired from commercial suppliers without any further purification. ^{1}H NMR spectra were obtained on 300 or 500 MHz spectrometers at room temperature, whereas ^{13}C NMR spectra were obtained on 75 or 125 MHz and ^{19}F NMR spectra were obtained at 282 MHz. ^{1}H NMR chemical shifts were determined relative to internal $(CH_3)_4Si$ (TMS) at δ 0.00 ppm. ^{13}C NMR chemical shifts were determined relative to the signal of the solvent: $CDCl_3$ δ 77.16 ppm. ^{19}F NMR chemical shifts were determined relative to $CFCl_3$ at δ 0.00 ppm. Chemical shifts (δ) were reported in ppm and coupling constants are reported in Hertz. The multiplicities are abbreviated as follows: s = singlet, d = doublet, t = triplet, m = multiplet, dd = doublet of doublets, and so forth. Mass spectra were obtained on a mass spectrometer. ^{18}F-CHL-2205 was purified with a Waters XSelect HSS T3 OBD™ Prep Column (5μm, 10 × 250 mm) with a flow rate of 5 mL/min with acetonitrile/H2O (v/v = 50/50, containing 0.1% NEt_3) as the eluting solvent. The UV detector was used at a wavelength of 254 nm. The product was collected and diluted with 10 mL of water and loaded onto activated Sep-Pak light C18 (Waters cat. No. WAT023501). After the Sep-Pak was washed with water (10 mL), ^{18}F-CHL-2205 was eluted with ethanol (0.5 mL). The resulting solution was formulated in saline (5% ethanol) for biological studies. The chemical and radiochemical purity were measured by use of an analytical HPLC (XBridge, C18 column, 5 μm, 4.6 mm×100 mm) with an eluent of CH_3CN/H_2O (50/50, v/v) at a flow rate of 1.0 mL/min and a UV detector wavelength of 254 nm was used.

Structure-activity relationship study

With the goal to develop a potent and selective CYP46A1 inhibitor suitable for radiolabeling (tritiation and radiofluorination) and translation PET imaging studies, we designed a series of inhibitor candidates with communal 4-phenyl-5-(piperazin-1-yl)pyrimidine scaffold based on our first-generation compound *N*-benzyl-4-(4-phenylpyrimidin-5-yl)piperazine-1-carboxamide, compound A (Chen et al., *Bioorg Med Chem Lett*, 2020), and soticlestat (Koike et al., *J Med Chem*, 2021). As shown in **Fig. S1**, compound A showed promising potency and was radiolabled by the [^{11}C]CO2 fixation method in high yield (21%) and high molar activity (>37 GBq/μmol). In our second iteration of medicinal chemistry, we found the switch from urea to carbamate core decreased the binding affinity (compound B, K_i=1.70 nM and compound C, K_i=3.76 nM) with good tolerance of the fluorine substituent on the terminal phenyl group of southwestern region. However, we didn't pursue the radiolabeling of these two compounds because of the similarity to compound A, which has low brain uptake (<0.4 SUV) in rats by PET. In our third iteration, fluorine was migrated to the

other phenyl ring of northeastern region ('fluorine walk'). compound D and E were synthesized to replace urea/carbamate core with amide structure. We designed compound D with *N*-methyl substituent with the possibility of tritiation; however, it was soon abandoned due to suboptimal binding affinity of 22 nM, at least, unsuitable for PET imaging. Initially we hypothesized that the decrease of binding affinity was, in part, attributed to the 'fluorine walk' between phenyl groups, but it was proven to be invalid because compound E showed substantially increased binding affinity (K_i=0.37 nM). The inferior binding affinity of compound D was probably caused by *N*-methyl piperazine whereas fluorine on the phenyl ring of northeastern region was well tolerated. Due to the lack of labeling handle on compound E, for example, *N*-methyl, in our fourth iteration, we synthesized our target molecule CHL-2205, codenamed Cholestify, as a congener of compound D and E, with the formation of cyclopropyl- and methyl-disubstituted amide. The target showed excellent binding affinity (Ki = 0.26 nM) and amenability for both tritiation and radiofluorination.

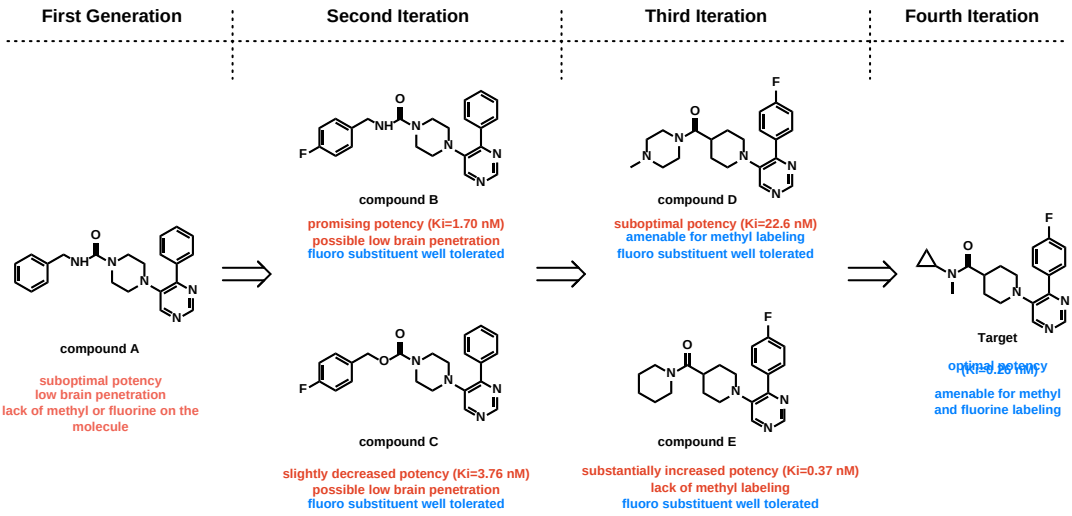

Fig. S1 Focused medicinal chemistry design with amenability for radiolabeling

Organic chemistry

*Synthesis of target compound N-cyclopropyl-1-(4-(4-fluorophenyl)pyrimidin-5-yl)-N-methylpiperidine-4-carboxamide (**CHL-2205**)*

A mixture of compound **1** (150.7 mg, 0.5 mmol), *N*-methylcyclopropanamine (46.2 mg, 0.65 mmol), HATU (1-[Bis(dimethylamino)methylene]-1H-1,2,3-triazolo[4,5-b]pyridinium 3-oxide hexafluorophosphate, Hexafluorophosphate Azabenzotriazole Tetramethyl Uronium, 247.1 mg, 0.65 mmol), DIPEA (*N*,*N*-diisopropylethylamine, 193.9 mg, 1.5 mmol) and DMF (3.3 mL) was stirred at room temperature for 16 h. The mixture was diluted with water and extracted with ethyl acetate. The organic layer was washed with water and brine, dried over $MgSO_4$, and concentrated.

The residue was purified with silica gel column chromatography to give compound **CHL-2205** in 85% yield (177 mg) as a yellow solid. ^{1}H NMR (300 MHz, $CDCl_3$) δ 8.92 (s, 1H), 8.70–8.30 (m, 1H), 8.18–8.12 (m, 2H), 7.16 (t, *J* = 8.7 Hz, 2H), 3.31–3.27 (m, 2H), 3.09 (m, 1H), 2.92 (s, 3H), 2.71–2.64 (m, 3H), 1.89 (qd, *J* = 12.1, *J* = 3.9 Hz, 2H), 1.72–1.68 (m, 2H), 0.93–0.71 (m, 4H). ^{19}F NMR (282 MHz, $CDCl_3$) δ -106.2 (m, 1F). ^{13}C NMR (75 MHz, $CDCl_3$) δ 177.5, 163.9 (d, *J* = 249.0 Hz), 156.9, 152.2, 146.7, 134.0, 130.5 (d, *J* = 8.5 Hz), 115.8 (d, *J* = 21.6 Hz), 50.7, 39.0, 34.5, 31.1, 28.5, 9.2.

*Synthesis of compound N-cyclopropyl-1-(4-(4-iodophenyl)pyrimidin-5-yl)-N-methylpiperidine-4-carboxamide (**3**)*

Compound **3** was prepared via the same procedure that described for **CHL-2205** in 57% yield as a yellow solid, except that compound **2** was used instead of compound **1**. ^{1}H NMR (500 MHz, $CDCl_3$) δ 8.89 (s, 1H), 8.42 (s, 1H), 7.88 (d, *J* = 8.5 Hz, 2H), 7.82 (d, *J* = 6.5 Hz, 2H), 3.30–3.28 (m, 2H), 3.09 (m, 1H), 2.92 (s, 3H), 2.70–2.65 (m, 3H), 1.88 (qd, *J* = 12.5, *J* = 3.5 Hz, 2H), 1.72–1.70 (m, 2H), 0.90–0.88 (m, 2H), 0.76–0.73 (m, 2H). ^{13}C NMR (125 MHz, $CDCl_3$) δ 177.5, 162.6, 156.5, 152.7, 147.3, 144.2, 137.9, 137.4, 129.9, 96.5, 50.7, 38.9, 34.5, 31.1, 28.5, 9.1. MS (ESI) m/z: 463.4 ($M + H^+$).

*Synthesis of compound N-cyclopropyl-N-methyl-1-(4-(4-(4,4,5,5-tetramethyl-1,3,2-dioxaborolan-2-yl)phenyl)pyrimidin-5-yl)piperidine-4-carboxamide (**4**)*

To a mixture of compound **3** (204 mg, 0.5 mmol), $Pd(dppf)Cl_2$ (14.5 mg, 0.02 mmol), Bis(Pinacolato)diboron (381 mg, 1.5 mmol), NaOAc (123 mg, 1.5 mg), DMF (2.5 mL) was added. The mixture was heated at 120°C for 3 h under N_2 atmosphere. The mixture was diluted with water and extracted with ethyl acetate. The organic layer was washed with water and brine, dried over $MgSO_4$, and concentrated. The residue was purified with silica gel column chromatography to give compound **4** in 70% yield (161 mg) as a yellow solid. ^{1}H NMR (500 MHz, $CDCl_3$) δ 8.91 (s, 1H), 8.41 (s, 1H), 8.08 (d, *J* = 8.0 Hz, 2H), 7.91 (d, *J* = 8.5 Hz, 2H), 3.31–3.29 (m, 2H), 3.07 (m, 1H), 3.08 (s, 3H), 2.71–2.64 (m, 3H), 1.92–1.86 (m, 2H), 1.68–1.66 (m, 2H), 1.37 (s, 12H), 0.89–0.88 (m, 2H), 0.74 (m, 2H). ^{13}C NMR (125 MHz, $CDCl_3$) δ 177.6, 157.5, 152.3, 146.8, 144.3, 140.5, 135.0, 127.3, 84.0, 50.6, 38.9, 34.4, 31.1, 28.4, 9.1. MS (ESI) m/z: 462.9 ($M + H^+$).

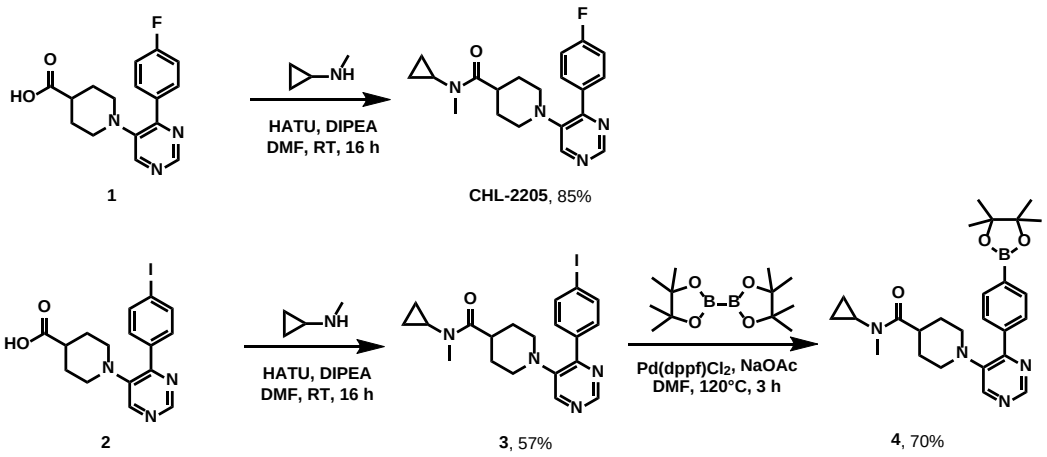

Fig. S2. Syntheses of **CHL-2205**, and borate precursor **4**.

Radiochemistry ^{18}F and ^{3}H

^{18}F-fluoride was from $H_2{}^{18}O$ via trapping on a Sep-Pak QMA Plus Light cartridge (Waters cat. No. 186004540) and subsequent elution from the cartridge with a solution of Et_4NHCO3 (1 mg) in MeOH (1 mL). The resulting solution was dried at 110 °C with a helium flow. Subsequently, a solution of borate precursor **4** (2 mg) and $[Cu(Py)_4OTf_2]$ (6 mg) in dry-DMA/nBuOH (200/100 μL) was added, and the reaction vial was heated at 110 °C for 20 min without the cap of the vial. After cooling the reaction mixture to ambient temperature, water (8 mL) was added and the resulting mixture passed through a Sep-Pak light C18 (Waters cat. No. WAT023501). After washing Sep-Pak light C18 with 10 mL water, the product was eluted with acetonitrile (1 mL). Water (2 mL) was added and the mixture was subjected to HPLC purification. ^{18}F-CHL-2205 was purified with a Waters XSelect HSS T3 OBD™ Prep Column (5μm, 10 × 250 mm) with a flow rate of 5 mL/min with acetonitrile/H_2O (v/v = 50/50, containing 0.1% NEt_3) as the eluting solvent. The UV detector was used at a wavelength of 254 nm. The product was collected and diluted with 10 mL of water and loaded onto activated Sep-Pak light C18 (Waters cat. No. WAT023501). After the Sep-Pak was washed with water (10 mL), ^{18}F-CHL-2205 was eluted with ethanol (0.5 mL). The average radiochemical yield was greater than 20% (n>20) with high molar activity (>1 Ci/μmol). The resulting solution was formulated in saline (5% ethanol) for biological studies. The chemical and radiochemical purity (>95%) were measured by use of an analytical HPLC (XBridge, C18 column, 5 μm, 4.6 mm×100 mm) with an eluent of CH_3CN/H_2O (50/50, v/v) at a flow rate of 1.0 mL/min and a UV detector wavelength of 254 nm was used.

^{3}H-CHL-2205 was synthesized via *N*-alkylation using ^{3}H-MeI (**Fig. S3**). To a solution of the amide precursor in DMF (3 mg/mL) was added NaH (1 eq.) at 0°C. The reaction mixture was allowed to

come to room temperature and ^{3}H-MeI was added. The resulting solution was stirred for 60 min at ambient temperature and subsequently quenched with ice cold water. HPLC purification gave the desired product, which was confirmed by co-injection and by scintillation counter, in an excellent radiochemical purity >99% and a molar activity of 2.79 TBq/mmol.

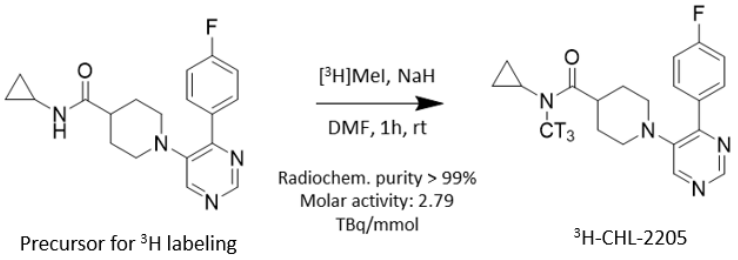

Fig. S3: Radiosynthesis of ^{3}H-CHL-2205.

Radioligand binding assay

To assess the binding affinity of ^{3}H-CHL-2205 towards CYP46A1, competitive radioligand binding assays using ^{3}H-CHL-2205 and the non-radioactive reference were conducted. Non-specific compound was dissolved in DMSO (10 mM) and stored frozen at - 20 °C. On the day of the assay, the compound was thawed and diluted with assay buffer to 5 x final maximal assay concentration. Rat brain regions were dissected out and homogenized in approximately 20 volumes ice cold buffer (50 mM Tris; 5 mM MgCl2; 5 mM EDTA; protease inhibitor cocktail). After a low-speed spin (100 x g) to remove tissue pieces, the supernatant was transferred to a fresh tube and centrifuged at 17,000 x g for 10 minutes at 4 °C to pellet the membranes. The pellet was resuspended in fresh buffer and centrifuged a second time. The pellet from the second spin was resuspended in buffer (50 mM Tris, 5 mM MgCl2, 0.1 mM EDTA) containing 10% sucrose as a cryoprotectant, divided into aliquots, frozen and stored at -80 °C. A sample of the washed membrane preparation was analyzed for protein content using the Pierce® BCA assay. Radioligand binding assays were carried out in 96-well plates in a final volume of 250 µL per well. To each well was added 150 µL membrane, 50 µL non-specific compound in buffer (or buffer alone) and 50 µL radioligand in buffer. The plate was incubated at 30 °C for 60 minutes with gentle agitation. The incubation was stopped by vacuum filtration onto presoaked (incubation buffer) GF/C filters using a 96-well FilterMate™ harvester, followed by five washes with ice-cold wash buffer. Filters were then dried under a warm air stream, sealed in polyethylene, scintillation cocktail added and the radioactivity counted in a Wallac® TriLux 1450 MicroBeta counter. For each concentration of drug, non-specific binding was subtracted from total binding to give specific binding. Data was

fitted using the non-linear curve fitting routines in Prism® (Graphpad Software Inc) to determine the dissociation constant (K_D) (**Fig. S4A and 4B**).

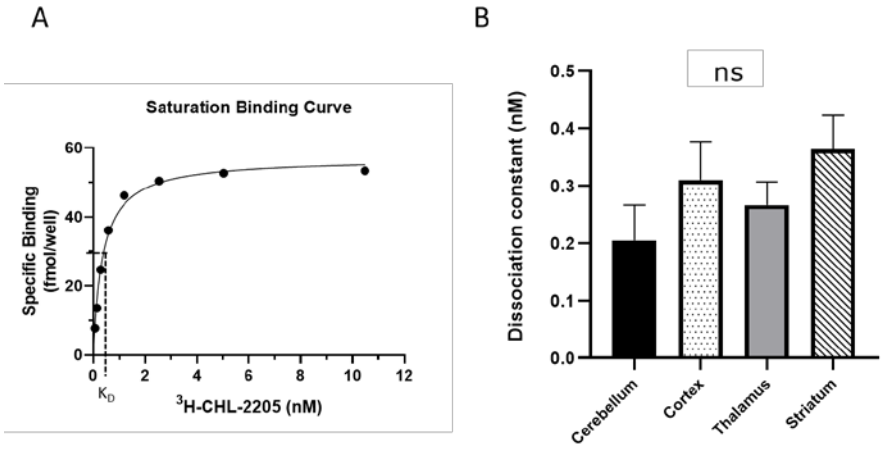

Fig. S4: Radioligand binding assays with ^{3}H-CHL-2205. **A.** Representative saturation binding curve with rat brain tissue homogenates. **B**. K_D determination on rat brain homogenates using different regions.

Selectivity screening

CHL-2205 was screened against a panel of 49 major CNS targets and proved to be highly selective. There was no significant interaction at a testing concentration of 10 µM, which corroborates autoradiographic findings with ^{18}F-CHL-2205 using CYP46A1 knock-out mouse brains (main manuscript).

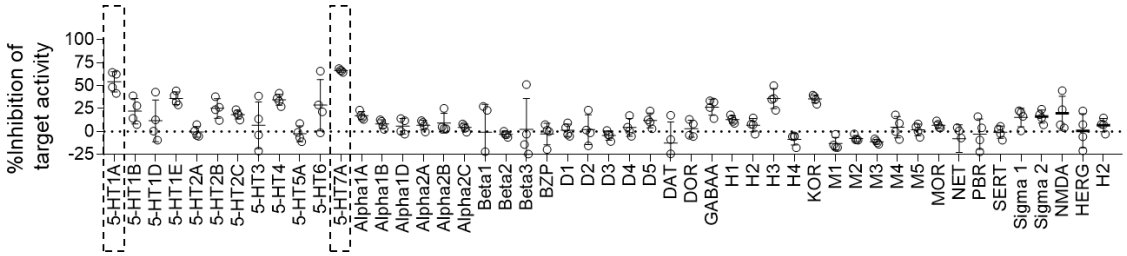

Target	Seconday Assay Ki [nM]
5-HT1A	3951 ± 1481
5-HT7A	2121 ± 343

Fig. S5: Off-target screening for CHL-2205 against 49 major central nervous system (CNS) targets. Primary assay showed no significant interactions at a CHL-2205 concentration of 10 µM.

Nonetheless, secondary radioligand binding assays were performed for the two targets with highest percentage of inhibition on primary screening, namely, 5-HT1A and 5-HT7A. The analysis revealed low-affinity Ki values of 3951 ± 1481 nM for 5-HT1A and 2121 ± 343 nM for 5-HT7A, respectively.

In vitro autoradiography

Rodent and NHP post-mortem brain tissue was embedded in Tissue-Tek® (O.C.T.). Sections of 10-20 µm thickness were prepared on a cryostat, mounted to glass slides and stored at -80 °C until further use. Prior to in vitro autoradiography experiments, brain sections were initially thawed for 10 min on ice and subsequently preconditioned for 10 min in the assay buffer (pH 7.4) containing 50 mM TRIS and 0.1-1% fatty acid free bovine serum albumin (BSA) at ambient temperature. Upon drying, the tissue sections were incubated with 1 mL of the respective ^{18}F-CHL-2205 solution (0.5-2 nM) for 20-30 minutes at 25 °C. For CYP46A1-blockade, 1 µM of soticlestat (or voriconazole) was added to the radiotracer solution. The brain sections were washed for 2x2 min in the washing buffer (pH 7.4) containing 50 mM TRIS and further dipped twice in distilled water, subsequently dried and exposed to a phosphor imager plate for 60 minutes. The films were scanned and images were analyzed using ImageQuant TL 8.1. A remarkable tracer specificity and selectivity for CYP46A1 was observed on autoradiograms of the rodent and NHP brain. Indeed, ^{18}F-CHL-2205 revealed a high selectivity to the CYP46A1-expressing forebrain in rodents and NHP brains (**Fig. S6**). Blockade studies were conducted with soticlestat or voriconazole in excess to elucidate their ability to compete with ^{18}F-CHL-2205 binding. The autoradiography findings suggested that ^{18}F-CHL-2205 specifically and selectively binds CYP46A1, thus rendering the probe potentially useful for non-invasive quantification of CYP46A1 abundancy by PET.

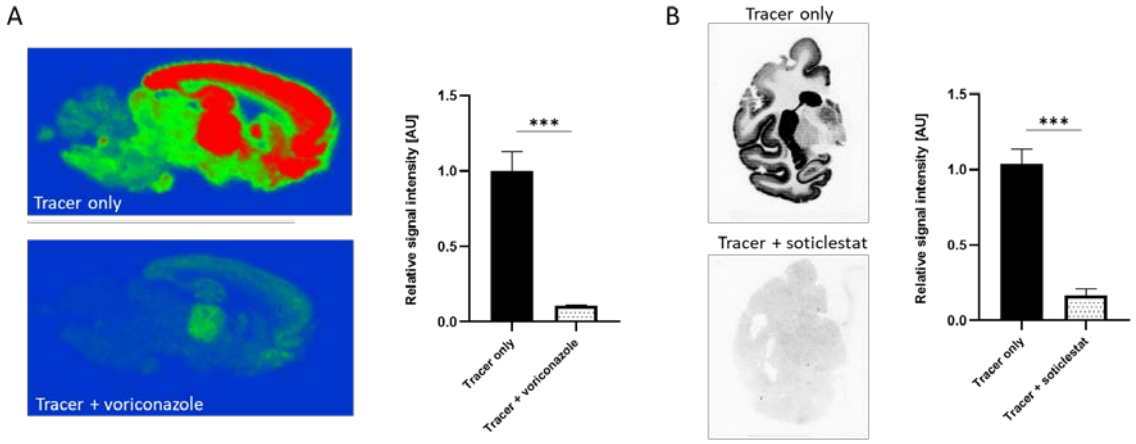

Fig. S6: In vitro autoradiography studies with ^{18}F-CHL-2205. **A.** Autoradiograms of the rat brain at baseline (upper) conditions and following blockade (lower) with excess 100 µM voriconazole. Quantification revealed specificity values up to 90% in rat brains. **B.** High regional selectivity at baseline (upper panel) and substantial signal reduction was further observed on NHP brain sections when blocked with excess 1 µM soticlestat (lower panel). Quantification revealed specificity values up to 80%.

Docking Studies

Three crystal structures of Cytochrome P450 (CYP46A1) were retrieved from the Protein Data Bank (PDB: 3MDT, 3MDM, and 7LRL). Each structure contained an inhibitor (voriconazole, thioperamide, or soticlestat), which was subsequently removed. The protein was prepared for docking using UCSF Chimera (v1.13.1), which involved the addition of hydrogen atoms, deletion of solvent, and assignment of AMBER ff14SB force field to protein residues. Docking was performed using AutoDock Vina (v.1.2.0).

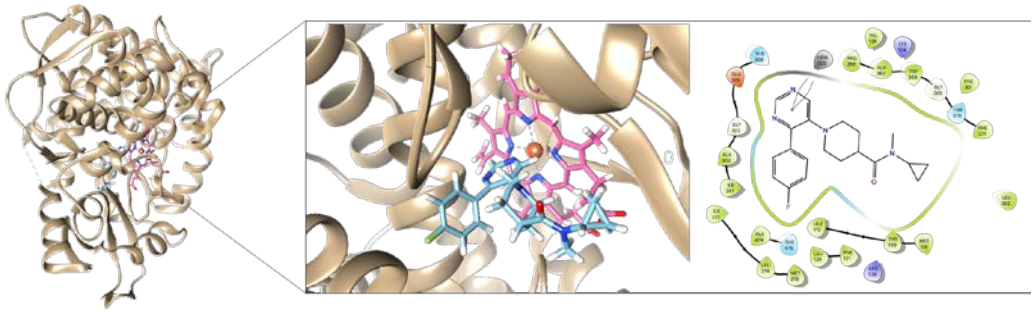

Fig. S7: Molecular docking findings of CHL-2205 (blue) to CYP46A1 (PDB:3MDT). Binding within the cavity was primarily composed of hydrophobic interactions, as well as one T-shaped pi-pi stacking with the protoporphyrin ring (pink).

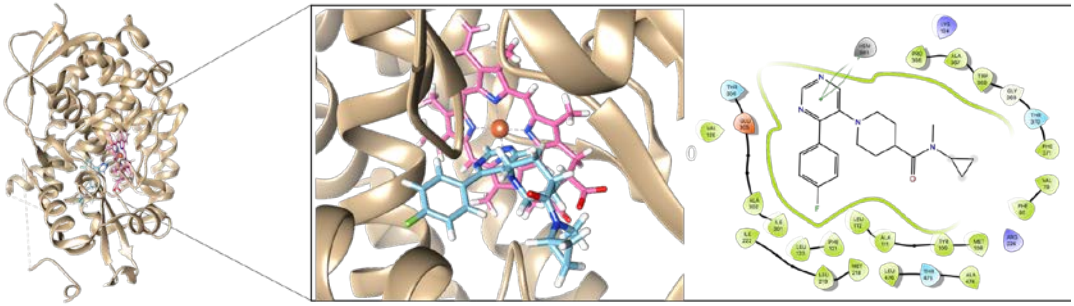

Fig. S8: Molecular docking findings of CHL-2205 (blue) to CYP46A1 (PDB:7LRL). Binding within the cavity was primarily composed of hydrophobic interactions, as well as one T-shaped pi-pi stacking with the protoporphyrin ring (pink).

Stability studies

Liver microsome stability experiments were conducted by mixing NADPH regenerating solutions (40 µL, 10 mmol/L in PBS), ^{18}F-CHL-2205 formulation in DMSO (10 µL, 200 µCi) and phosphate-buffered saline (340 µL, 1X). Mouse, rat, non-human primate and human liver microsomes (Sigma–Aldrich) were added after preincubation at 37 °C for 5 min. Subsequently, the samples were incubated at 37 °C for 30 min, followed by the addition of 400 µL ice cold MeCN to terminate the enzymatic reactions, as well as vortexing and centrifuging at 21,000×g for 5 min. The percentage of intact parent and radiometabolites was assessed by radioTLC using different eluent compositions of either hexane/EtOAc or DCM/MeOH. Commercially available (±)-verapamil hydrochloride was used as positive control. The percent of parent PET tracer is depicted in **Fig. S9**.

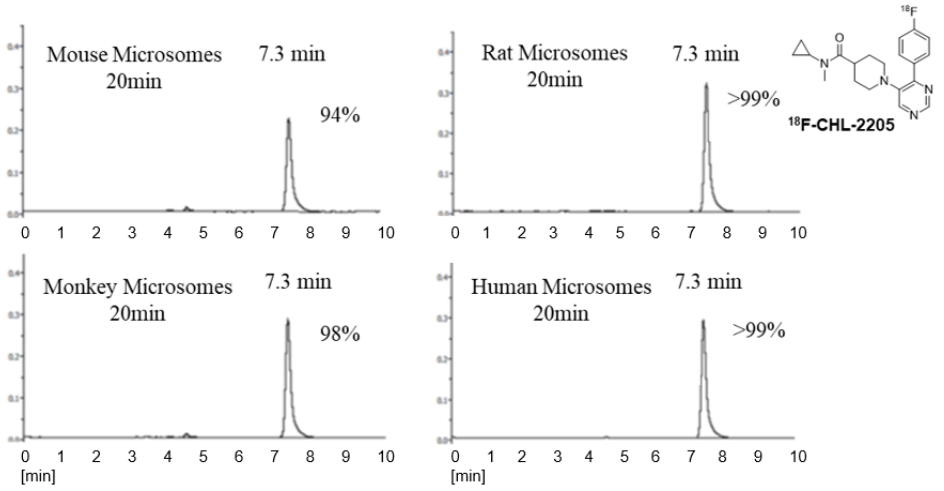

Fig. S9A: In vitro stability studies with ^{18}F-CHL-2205. Chromatograms after incubation with microsomes of mouse, rat, non-human primate (NHP) or human source.

Ex vivo brain uptake, brain metabolite study and whole-body dosimetry

Ex vivo brain uptake studies and whole-body dosimetry was conducted in CD1 mice (8 weeks, 25–30 g) that were maintained on a 12 h light/12 h dark cycle and provided water ad libitum. 50 µCi (1.85 MBq) of ^{18}F-CHL-2205 (100 µL) was injected intravenously to each mouse via the tail vein. At the time point of 5, 15, 30 and 60 min, mice (n = 4) were sacrificed by cervical dislocation and

the brains were collected and weighted. An automatic gamma counter (PerkinElmer, USA) was used for determining each organ's decay-corrected radioactivity. For dosimetry, additional time points included 180 and 360 min post tracer injection.

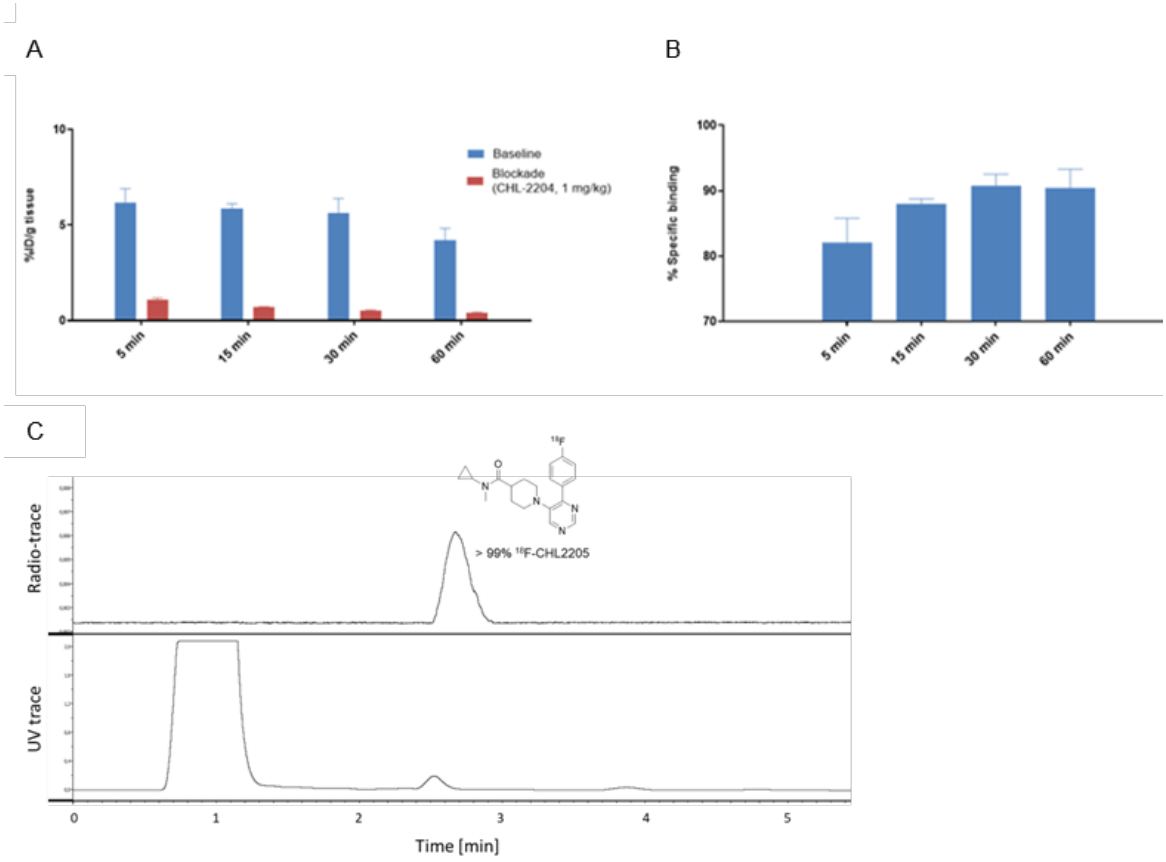

Fig. S10: Ex vivo brain uptake and metabolite study of ^{18}F-CHL-2205 in mice. **A.** Baseline vs. blocking with 1 mg/kg CHL-2205 at 5, 15, 30 and 60 min post tracer injection. **B.** Specific CYP46A1 binding in the mouse brain at different time points, calculated as follows: (baseline – blockade) / baseline * 100. **C**. Representative ex vivo metabolite study chromatogram following intravenous injection of ^{18}F-CHL-2205 into mice and subsequent analysis of brain homogenates at 30 min post injection.

Target Organ	Alpha	Beta	Photon	Total	EDE Cont.	ED Cont.
Adrenals	0.00E+00	1.15E-02	1.05E-02	2.20E-02	2.20E-02	2.03E-04
Brain	0.00E+00	3.32E-03	5.34E-03	8.67E-03	8.67E-03	8.67E-05
Breasts	0.00E+00	4.92E-03	6.00E-03	1.09E-02	1.09E-02	1.31E-03
Esophagus	0.00E+00	4.92E-03	6.80E-03	1.17E-02	1.17E-02	4.69E-04
Eyes	0.00E+00	4.92E-03	6.42E-03	1.13E-02	0.00E+00	0.00E+00
Gallbladder Wall	0.00E+00	4.92E-03	1.08E-02	1.57E-02	1.57E-02	1.45E-04
Left colon	0.00E+00	4.92E-03	1.05E-02	1.55E-02	1.55E-02	7.50E-04
Small Intestine	0.00E+00	1.13E-02	1.05E-02	2.19E-02	2.19E-02	2.02E-04
Stomach Wall	0.00E+00	6.07E-03	8.92E-03	1.50E-02	1.50E-02	1.80E-03
Right colon	0.00E+00	4.93E-03	1.11E-02	1.61E-02	1.61E-02	7.80E-04
Rectum	0.00E+00	4.92E-03	1.07E-02	1.57E-02	1.57E-02	3.60E-04
Heart Wall	0.00E+00	1.09E-03	7.33E-03	8.41E-03	8.41E-03	7.76E-05
Kidneys	0.00E+00	4.19E-03	9.32E-03	1.35E-02	1.35E-02	1.25E-04
Liver	0.00E+00	8.20E-03	1.10E-02	1.92E-02	1.93E-02	7.70E-04
Lungs	0.00E+00	2.26E-03	7.70E-03	9.96E-03	1.00E-02	1.20E-03
Ovaries	0.00E+00	4.92E-03	1.10E-02	1.59E-02	1.59E-02	6.37E-04
Pancreas	0.00E+00	9.96E-04	1.01E-02	1.11E-02	1.12E-02	1.03E-04
Salivary Glands	0.00E+00	4.92E-03	7.37E-03	1.23E-02	1.23E-02	1.23E-04
Red Marrow	0.00E+00	3.50E-03	8.71E-03	1.22E-02	1.23E-02	1.47E-03
Osteogenic Cells	0.00E+00	6.30E-03	9.06E-03	1.54E-02	1.54E-02	1.54E-04
Spleen	0.00E+00	6.18E-04	8.07E-03	8.68E-03	8.69E-03	8.02E-05
Thymus	0.00E+00	4.95E-03	8.05E-03	1.30E-02	1.30E-02	1.20E-04
Thyroid	0.00E+00	4.92E-03	7.36E-03	1.23E-02	1.23E-02	4.91E-04
Urinary Bladder Wall	0.00E+00	4.92E-03	8.12E-03	1.30E-02	1.31E-02	5.22E-04
Uterus	0.00E+00	4.30E-04	9.92E-03	1.03E-02	1.03E-02	4.78E-05
Total Body	0.00E+00	5.49E-03	7.85E-03	1.33E-02	0.00E+00	0.00E+00
Effective Dose Equivalent (mSv/MBq)					0.329	
Effective Dose (mSv/MBq)						0.012

Effective dose for ^{18}F-FDG → 0.019 mSv/MBq

Fig. S11: Dosimetry of ^{18}F-CHL-2205 predicted from an extended ex vivo biodistribution study in mice. An effective dose of 0.012 mSv/MBq was predicted, which is below the typical effective dose for an ^{18}F-fluorodeoxyglucose (^{18}F-FDG) scan.

Small-animal PET/CT in mice

Dynamic PET imaging was conducted using a PET/CT scanner (Sofie, MA, USA). Isoflurane (2% v/v) in a 1:1 mixture of air/oxygen were used for anesthesia. ^{18}F-CHL-2205 was intravenously administrated into the mouse via a preinstalled catheter, and mouse brain PET scans were acquired for 60 min in a dynamic 3D list mode. PMOD software (version 4.2) was used to generate the representative PET images and analyze the TACs from a template of predefined volumes of interest (VOI) in the cortex, striatum, hippocampus and cerebellum.

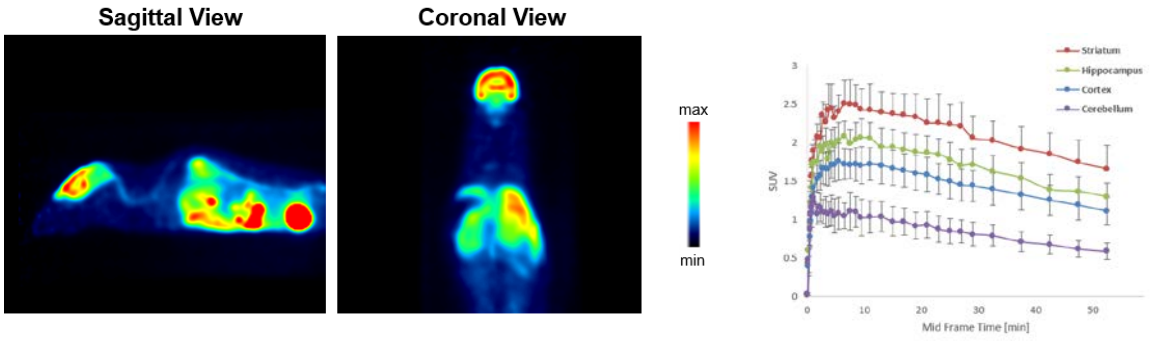

Fig. S12: Positron emission tomography (PET) imaging with ^{18}F-CHL-2205 in mice. Representative sagittal and coronal views are presented. Time-activity curves (TACs) revealed

highest tracer uptake in the striatum, followed by hippocampus and cortex. Cerebellar uptake was the lowest, which is in accordance with CYP46A1 expression patterns.

Sterol analysis

Sterol measurements were conducted as previously validated by Griffith and co-workers. Frozen tissue sections (10µm) were dried in a vacuum desiccator for 15 min, prior to the addition of an internal standard mixture. Subsequently, cholesterol oxidase (0.264 units/mL in 50 mM KH2PO4, pH7) was added, and the samples were incubated at 37 °C for 1 h, after which the slide was removed and dried for 15 min. [$^2H_5$]GP (6.3 mg/mLof bromide salt in 70% methanol with 5% acetic acid was sprayed and the samples were incubated at 37 °C for 1 h. The slides were removed and dried *in vacuo* until LC-MS analysis. To analyze the sterol content, cholesterol oxidase spray step was omitted and [$^2H_0$]GP (5 mg/mL chloride salt, in 70% methanol with 5% acetic acid) was used for derivatization.

A

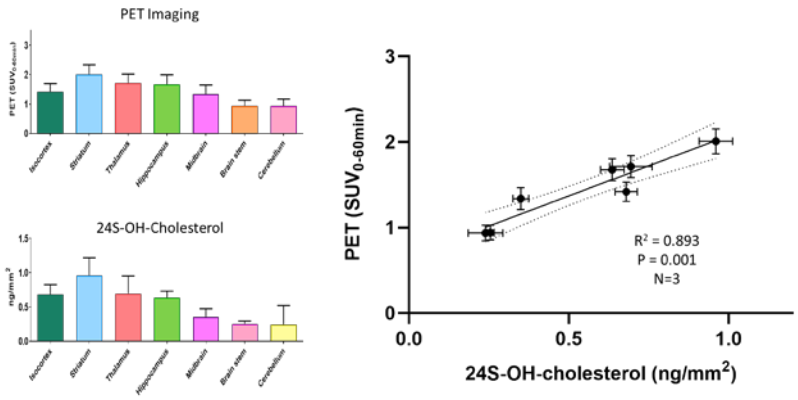

B

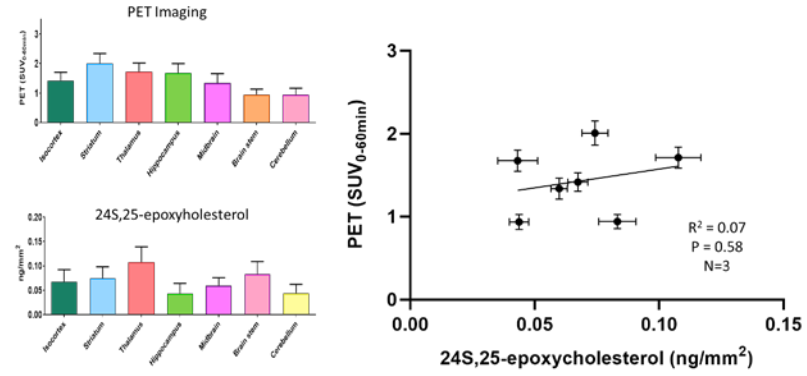

Fig. S13: Sterol analysis and comparison of PET signal with major brain cholesterol metabolites. **A**. Assessment for 24S-OH-cholesterol, which is formed only via CYP46A1 catalyzed metabolism

of cholesterol. **B**. Assessment for 24S,25-epoxycholesterol, which is formed via an alternative pathway involving other enzymes in the mammalian brain. The PET signal is significantly correlated with 24S-OH-cholesterol, but not with 24S,25-epoxycholesterol.

Target occupancy studies

For target occupancy studies, CYP46A1 inhibitor, soticlestat, was administered intravenously (iv) at the doses of either 0.0009, 0.0016, 0.014, 0.016, 0.05, 0.12, 0.32 and 0.34 mg/kg was injected iv, shortly prior to the injection of ^{18}F-CHL-2205. PET/CT and MR images were co-registered according to the method that was previously validated by McLaren et al. Time-activity curves (TACs) were derived from the respective volumes of interest (VOIs) and the area under the curve was used to estimate target occupancy, as previously reported.

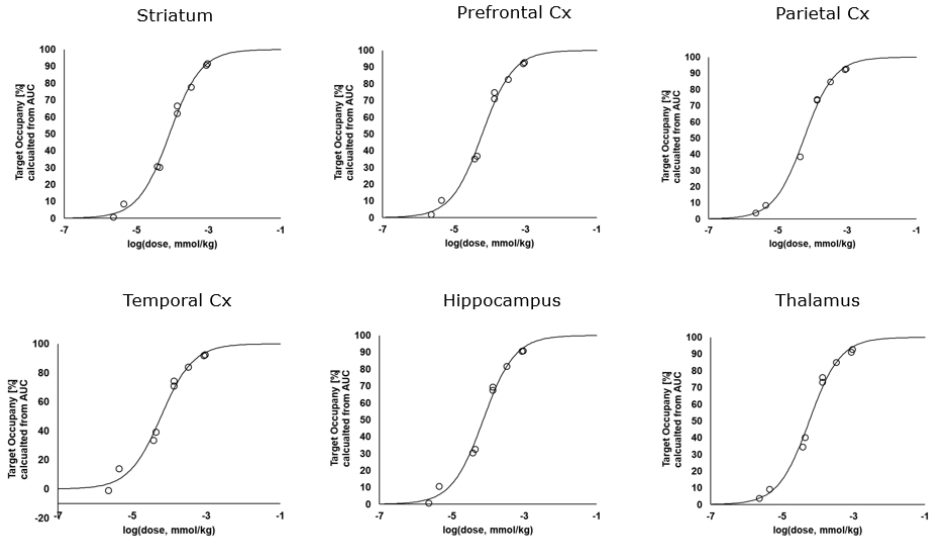

Fig. S14: Target occupancy of CYP46A1 inhibitor, soticlestat, as determined from PET imaging with ^{18}F-CHL-2205 in non-human primates.

Clinical study

Table S1: Demographics of the study population**.**

Subject	Age [Years]	Weight [kg]	Injected dose [MBq]	Sex
1	24	45.0	200.8	F
2	22	48.0	173.9	F
3	27	46.0	179.3	F
4	30	63.0	191.6	M
5	31	62.0	186.8	M
6	22	67.0	225.6	M
7	25	56.5	205.8	F
8	27	79.0	305.8	M

Table S2: Individual volumes of distribution (V_T) in selected brain regions and for all participants**.**

Subject	PFCx	TPCx	Th	Put	Cau	Hp	Pon	CC	Cb
2	7.27	6.75	6.04	10.72	9.20	5.73	2.97	2.78	2.95
3	7.30	7.75	6.20	11.24	8.94	5.11	3.90	2.34	3.10
4	6.07	5.84	4.84	9.23	6.60	4.07	2.59	2.37	2.26
5	5.51	5.85	4.42	7.79	6.16	4.45	2.74	1.72	2.16
6	6.01	5.71	4.32	9.20	7.28	4.09	2.50	2.23	2.12
7	7.51	8.06	6.22	11.83	9.47	5.58	3.93	2.80	3.66
8	6.25	6.80	5.40	9.56	7.20	5.08	3.37	3.13	2.48

***** No kinetic modeling data available for subject 1 due to lack of appropriate input function. PFCx, prefrontal cortex; TPCx, temporal cortex ; Th, thalamus; Put, putamen, Cau, caudate; Hp, hippocampus; CC, corpus callosum; Cb, cerebellum.